# Quantum Monte Carlo study of tunneling diffusion in a dissipative multistate system

C. H. Mak and Reinhold Egger
*Department of Chemistry, University of Southern California, Los Angeles, California 90089-0482*
(Received 15 October 1993)

Real-time quantum Monte Carlo (QMC) methods have been used to study diffusion on a one-dimensional tight-binding lattice in a dissipative environment with Ohmic friction. For this system, the inherent sign problem of real-time QMC methods can be substantially reduced by employing a partial summation scheme, allowing direct calculations of long-time transport properties. At very low temperatures, the system undergoes a transition from a coherent transport mechanism to an incoherent mechanism as the Kondo parameter $K$ goes through 1. For $0 < K < 1$, perturbation theory which predicts a $T^{2K-1}$ power-law temperature dependence for the diffusion coefficient $D$ is grossly incorrect for low temperatures. Instead, $D(T \to 0) = 0$ for $0 < K < \frac{1}{2}$, and with increasing temperature $D$ goes through a pronounced maximum. This maximum disappears for $K > \frac{1}{2}$ and D increases monotonically with increasing temperature. For all $K < 1$, perturbation theory becomes exact at sufficiently high temperatures, indicating that the transport mechanism eventually becomes incoherent. For $K > 1$, perturbation theory is exact for all temperatures, and transport is always incoherent.

PACS number(s): 05.30.−d, 03.65.Bz, 73.40.Gk

## I. INTRODUCTION

The study of tunneling dynamics of quantum systems in condensed phase is important in many areas of physics and chemistry. In these systems, to correctly describe the dissipative effects of the condensed phase environment, a heat bath has to be included, which severely limits the usefulness of conventional quantum-mechanical methods such as basis-set techniques. A powerful alternative for dealing with these open quantum systems is the path-integral approach of Feynman [1]. Making use of Feynman path integrals, Caldeira and Leggett [2] constructed models of open quantum systems representing the bath as an infinite collection of harmonic oscillators which are then allowed to couple to the quantum system linearly. Because of the linear system-bath coupling and the harmonic nature of the bath modes, the entire bath can be traced out according to the influence functional method of Feynman and Vernon [3], leaving an effectively one-dimensional system dressed with nonlocal self-interactions.

Many path-integral studies of condensed phase tunneling systems focused on the dissipative two-level system commonly known as the spin-boson model [4] first used to describe the motion of magnetic flux in rf superconducting quantum interference devices. Interestingly, the same spin-boson model has found wide applications to many other areas of physics and chemistry. To mention two examples, it has been used to study tunneling of charged particles coupled to conduction electrons in a metal [5], as well as the electron tunneling rate constant in many chemical and biological electron transfer reactions [6]. In the past, we have studied many aspects of the spin-boson model using real-time quantum Monte Carlo (QMC) methods, incorporating a filtering scheme for discrete-state systems which partially circumvents the sign problem inherent in all real-time path-integral calculations. These QMC methods carry out the path summation (after discretizing the action) in a stochastic manner, and the sign problem arises because paths carrying different phases interfere with each other. The filtering scheme we have employed previously [7] simply steers the Monte Carlo (MC) trajectory away from regions of destructive interference, thereby making the path summation better conditioned. In many cases these simulation techniques have confirmed predictions of analytical theories, in particular, the noninteracting-blip approximation [4], and in others they have provided detailed information about the dynamics of the spin-boson model in many widely differing regions of the parameter space [7–10].

In this paper, we will use a variant of the filtering scheme to simulate tunneling transport on a dissipative one-dimensional lattice with an infinite number of states. From a computational point of view, the most significant difference between the two-state and the multistate system is the path space volume that needs to be sampled. Because the number of paths grows with the number of states $N_s$ like $N_s^{\gamma(t)}$, where $\gamma(t)$ is some linear function of the real time $t$, the computational problem is much more demanding for a multistate system compared to a two-state system. However, this aspect of the problem by itself is not the most detrimental, because the action places constraints on the paths and effectively limits the number of allowed paths to a much smaller set. Furthermore, if the action is purely real valued, as in an imaginary-time calculation, the path summation could be carried out without much difficulty. The main problem arises when the weights of the paths are not positive definite, as is required for computing dynamics. Our past experience suggests that the severity of the sign problem (measured by the magnitude of the noise compared to the signal) grows exponentially with the effective size of path

 

space [7]. Therefore, a moderate increase in the number of states may lead to an entirely uncontrollable sign problem. However, we will show in this paper that efficient methods can be constructed to circumvent the sign problem, allowing us to extract the diffusion coefficient, which is an intrinsically long-time large-length-scale property, from the multistate system. The calculation of the linear mobility using a similar QMC method has also been addressed recently [11].

The model we are considering here is most relevant to quantum effects in the current-voltage characteristics of a small Josephson junction [12], but it can also serve as an idealized model for the diffusion of a quantum particle on the surface of a single-crystal or among interstitials inside a crystal [13,14], especially that of a charged particle in a metal [5], or for electron or hole transport in a quantum well structure within the one-band approximation [15]. The same model can also be used to study electron transfer in a charge-transport chain [16]. Finally, this multistate system can be related to the Luttinger liquid model for the conductance between two one-dimensional quantum wires connected by a weak link via a formally exact mapping [11].

The dissipative multistate system has been the subject of intense studies during the past decade [17–19,21,20,22–26]. Much of the physics of this model has been unraveled by renormalization-group methods and by an extremely useful duality transformation [17–19]. The duality links the (discrete) tight-binding problem studied here to the (extended) weak corrugation model describing a particle in a cosine potential and thereby imposes some interesting constraints on the transport quantities of both models. These calculations showed that for zero temperature, the multistate system undergoes a phase transition from a delocalized to a self-trapped state. The dual weak corrugation model has been studied by Fisher and Zwerger [19] with the Feynman-Vernon technique. A similar treatment of the weak corrugation model based on the Keldysh technique has been given by Eckern and Pelzer [20]. Based on the duality transformation and the results for the weak corrugation model, Weiss *et al.* [21] have extracted much of the qualitative behavior of the mobility and the diffusion coefficient for the tight-binding model. We will rely heavily on the analycial methods developed in Ref. [21] in this work, which prove useful also in a numerical context.

The outline of this paper is as follows. In Sec. II, we define the multistate model studied here. Section III discusses perturbation theory results for the multistate system and its connection with the noninteracting-blip approximation. Section IV gives a description of the Monte Carlo algorithm for computing the diffusion coefficient. In Sec. V, we present QMC results and compare them to perturbation theory. Some final analyses and conclusions are given in Sec. VI. For completeness, the MC algorithm for computing the mobility under an external bias is also included in the Appendix.

## II. THE DISSIPATIVE MULTISTATE MODEL

In this paper we consider a one-dimensional infinite tight-binding lattice with the Hamiltonian

$$H = H_0 + H_B + H_I \ . \tag{2.1}$$

Here $H_0$ is the Hamiltonian for the bare multistate system

$$H_0 = -(\hbar\Delta/2)\sum_j (c_j^\dagger c_{j+1} + c_{j+1}^\dagger c_j) - \hbar\epsilon q \ , \tag{2.2}$$

where $c_j^\dagger$ creates a particle on site $j$, and $\epsilon$ is an external bias. The operator $q$ measures the position of the particle on the lattice (in units of the lattice constant $a$)

$$q = \sum_j j n_j \ , \tag{2.3}$$

where $n_j = c_j^+ c_j$ is the number operator. Although we have employed creation and annihilation operators to define the multistate system, the commutation relationships for these operators are irrelevant here, since we confine ourselves to systems with only one particle in this work.

The bath is represented by a set of linearly responding (harmonic) modes $\{x_\alpha\}$

$$H_B = \sum_\alpha \frac{p_\alpha^2}{2m_\alpha} + \tfrac{1}{2} m_\alpha \omega_\alpha^2 x_\alpha^2 \ , \tag{2.4}$$

and the system-bath interaction is assumed to be of the form

$$H_I = \sum_\alpha -C_\alpha x_\alpha a q + \frac{C_\alpha^2}{2m_\alpha\omega_\alpha^2} a^2 q^2 \ . \tag{2.5}$$

A potential renormalization term has been added to $H_I$ to avoid an artificial shift in the potential of the bare system due to the inclusion of dissipation [4]. For the model Hamiltonian (2.1), the effects of the bath are captured entirely by the spectral density [2]

$$J(\omega) = \frac{\pi}{2}\sum_\alpha \frac{C_\alpha^2}{m_\alpha\omega_\alpha}\,\delta(\omega-\omega_\alpha) \ . \tag{2.6}$$

In this paper, we will consider specifically the case of frequency-independent damping (Ohmic dissipation) with a high-frequency exponential cutoff

$$J(\omega) = (2\pi\hbar K/a^2)\,\omega\exp(-\omega/\omega_c) \ , \tag{2.7}$$

where $K$ is the dimensionless system-bath coupling constant commonly referred to as the Kondo parameter [4,5].

One transport property of interest for this model is the diffusion coefficient $D$. When the system dynamics is diffusive, $D$ is related to the equilibrium correlation function of the displacement under zero external field ($\epsilon = 0$) by

$$D = a^2 \lim_{t\to\infty} \langle [q(t) - q(0)]^2\rangle / 2dt \ , \tag{2.8}$$

where $d$ is the dimensionality of the system, which is equal to one here, and the angular brackets denote an equilibrium Boltzmann average over the initial state of the system.

In this work, we will not consider genuine equilib-

rium experiments. Instead we will study a closely related situation—that assuming a factorized initial state [3]. In this experiment, the particle was prepared at time $t = 0$ at the origin $j = 0$, with the bath itself in a thermal distribution characterized by a temperature $T$. The dynamical quantity of interest is now the occupation probability $P_j(t)$ for finding the particle at site $j$ after some time $t$. In this experiment, the diffusion coefficient under $\epsilon = 0$ is given by

$$D = a^2 \lim_{t\to\infty} \langle q^2(t)\rangle/2dt \,, \tag{2.9}$$

where the mean squared displacement is related to the time-dependent occupation probabilities by $\langle q^2(t)\rangle = \sum_j j^2 P_j(t)$. It is important to point out that not all dynamical quantities observed in this type of experiment are necessarily identical to those observed in equilibrium experiments, particularly those involving short-time transient behaviors. However, for the present study, since the diffusion coefficient depends only on the long-time dynamics of the system, the precise manner in which the system was prepared initially is not important [23], and both initial conditions should yield the same diffusion coefficient. Since the factorized initial condition is somewhat easier to treat numerically, we only consider factorized initial states in this work.

The time-dependent occupation probability of observing the particle at site $n$ can be obtained using the influence functional method of Feynman and Vernon [3]

$$P_n(t) = \int \mathcal{D}q \int \mathcal{D}q' \exp\{S_0[q(\tau)] + S_0'[q'(\tau)]\} \times \mathcal{F}[q(\tau), q'(\tau)] \,, \tag{2.10}$$

where the path integrals denote a sum over all forward- and reverse-time paths $q(\tau), q'(\tau)$ satisfying the boundary conditions $q(0) = q'(0) = 0$ and $q(t) = q'(t) = n$. In Eq. (2.10), $S_0$ and $S_0'$ denote the free actions of the forward- and reverse-time paths, respectively, and $\mathcal{F}$ is the influence functional

$$\mathcal{F}[q(\tau), q'(\tau)] = \exp\left( - \int_0^t d\tau \int_0^\tau d\tau' \, [q(\tau) - q'(\tau)][L(\tau - \tau')q(\tau') - L^*(\tau - \tau')q'(\tau')] - \frac{i\mu}{2} \int_0^t d\tau [q(\tau)^2 - q'(\tau)^2] \right) , \tag{2.11}$$

where $L(\tau)$ denotes the response function of the bath weighted by the spectral density,

$$L(\tau) = \frac{a^2}{\pi\hbar} \int_0^\infty d\omega \, J(\omega) \frac{\cosh([\beta\hbar/2 - i\tau]\omega)}{\sinh(\beta\hbar\omega/2)} \,, \tag{2.12}$$

and the potential renormalization parameter is $\mu \equiv (2a^2/\pi\hbar) \int d\omega J(\omega)/\omega$.

Switching to the sum and difference coordinates

$$x(\tau) \equiv \frac{q(\tau) + q'(\tau)}{2} \,, \qquad y(\tau) \equiv q(\tau) - q'(\tau) \,, \tag{2.13}$$

and integrating by-parts twice, we obtain

$$\mathcal{F}[x(\tau), y(\tau)] = \exp\left( \int_0^t d\tau \int_0^\tau d\tau' \, [\dot{y}(\tau) S(\tau - \tau') \dot{y}(\tau') + 2i\dot{y}(\tau) R(\tau - \tau') \dot{x}(\tau')] \right) , \tag{2.14}$$

where $S$ and $R$ are the real and imaginary parts of $Q(\tau)$, which is related to the $L(\tau)$ function in Eq. (2.12) by $d^2Q(\tau)/d\tau^2 = L(\tau)$; for an Ohmic spectral density (2.7), this function can be evaluated exactly [9]. In terms of the sum and difference coordinates, the path-integral representation for $P_n(t)$ becomes

$$P_n(t) = \int \mathcal{D}x \int \mathcal{D}y \exp(\widetilde{S}_0[x(\tau), y(\tau)]) \, \mathcal{F}[x(\tau), y(\tau)] \,, \tag{2.15}$$

where we have collected the free actions for the forward- and reverse-time paths into a single action $\widetilde{S}_0$. The path integrals now entail a sum over all paths $x(\tau)$ and $y(\tau)$ [which are interdependent because of Eq. (2.13)] satisfying the boundary conditions $x(0) = y(0) = y(t) = 0$ and $x(t) = n$.

To obtain a path-integral expression for the mean squared displacement, one can introduce the generating functional

$$Z(\lambda, t) = \sum_{n=-\infty}^{\infty} e^{\lambda n} P_n(t) \,. \tag{2.16}$$

The mean squared displacement is obtained from the generating functional via

$$\langle q^2(t)\rangle = \partial^2 Z(\lambda, t)/\partial\lambda^2|_{\lambda=0} \,. \tag{2.17}$$

Equation (2.17) together with Eqs. (2.14)–(2.16) form the basis for both the analytical calculations and the numerical simulations discussed in the next sections.

## III. PERTURBATION THEORY AND THE NONINTERACTING BLIP APPROXIMATION

For high temperatures and/or strong damping, the transport of the particle proceeds by incoherent tunneling from one well to a neighboring well. The diffusion coefficient for such an incoherent stepwise transport can be computed in terms of a master equation describing the time-dependent occupational probability [22]. From a solution of the master equation, an expression for the diffusion coefficient can be derived in a straightforward manner as in classical diffusion theory, giving for $d = 1$

$$D = a^2\Gamma \,, \tag{3.1}$$

where $\Gamma$ is the stepwise forward rate. For this kind of

transport, the only difference between quantum and classical diffusion is the expression for the stepwise transfer rate that enters the master equation. For incoherent quantum diffusion, the quantum rate from the dissipative two-state system is used, whereas for classical diffusion, the Arrhenius rate is used. For a symmetric dissipative two-state system, the forward rate at high temperatures and/or strong dissipation is given by the golden rule formula

$$\Gamma_{\rm GR} = (\Delta/2)^2 \int_{-\infty}^{\infty} d\tau\, e^{-Q(\tau)} \,. \tag{3.2}$$

In view of this, the expression for $D$ in Eq. (3.1) appears to be simply the result of a perturbation theory to second order in the tunneling matrix element. However, Eq. (3.1) is more general than it appears. In the following, we will briefly describe how Eq. (3.1) emerges from a path-integral description of the system dynamics under a simple but powerful approximation commonly called the noninteracting-blip approximation (NIBA) [4]. The following discussion will follow closely that of Weiss *et al.* [21] and will also serve to set up the notations used in Sec. IV.

We begin by noticing that because of the tight-binding nature of our lattice model, the particle makes instantaneous transitions between neighboring wells. Since the two paths $q(\tau)$ and $q'(\tau)$ must end on the same site, they must make a total of $2m$ jumps, where $m = 0, 1, 2, \ldots$. Let the times at which these transitions occur be $t_1, t_2, \ldots, t_{2m}$. Changing variables from $q, q'$ to $x, y$ as in Eq. (2.13) one obtains

$$x(\tau) = \sum_{i=1}^{2m} x_i \Theta(\tau - t_i) \,, \qquad y(\tau) = \sum_{i=1}^{2m} y_i \Theta(\tau - t_i) \,, \tag{3.3}$$

where $\Theta$ is the Heaviside function, and now $x_i = \pm 1/2$ and $y_i = \pm 1$. There is no constraint on the relationship between $x_i$ and $y_i$ at the same time $t_i$. In terms of the "charges" [21] $\{x_i\}$ and $\{y_i\}$, the influence functional becomes

$$\mathcal{F}[x,y] = \exp\Bigg( \sum_{j=1}^{2m-1} \sum_{k=j+1}^{2m} y_k S(t_k - t_j) y_j + 2i \sum_{j=1}^{2m-1} \sum_{k=j+1}^{2m} y_k R(t_k - t_j) x_j \Bigg) \,. \tag{3.4}$$

The probability $P_n(t)$ is then obtained by first summing over all possible charge configurations $\{x_i\}$ and $\{y_i\}$ with the constraints $y(0) = x(0) = y(t) = 0$, $x(t) = n$, and $\sum_j y_j = 0$ for paths with $2m$ transitions, followed by a time-ordered integration over the possible transition times $\{t_1, t_2, \ldots, t_{2m}\}$, and finally a sum over all $m$.

Putting the expression for the influence functional Eq. (3.4) into the generating functional $Z(\lambda, t)$ and summing over all possible charge configurations for $\{x_i\}$, we obtain (for $\epsilon = 0$)

$$Z(\lambda,t) = \sum_{m=0}^{\infty} \Delta^{2m} \int_0^t \mathcal{D}_{2m}\{t_i\} {\sum_{\{y_i\}}}' \exp\left[ \sum_{j=1}^{2m-1} \sum_{k=j+1}^{2m} y_k S(t_k - t_j) y_j \right] \sinh\frac{\lambda}{2} \prod_{j=1}^{2m-1} \sinh\left[ \frac{\lambda}{2} + i \sum_{k=j+1}^{2m} y_k R(t_k - t_j) \right] \,, \tag{3.5}$$

where the prime on the $\{y_i\}$ summation indicates that the sum is subject to the constraint $\sum_j y_j = 0$ and the symbol $\int_0^t \mathcal{D}_{2m}\{t_j\}$ denotes the time-ordered integration over the transition times $\int_0^t dt_{2m} \int_0^{t_{2m}} dt_{2m-1} \cdots \int_0^{t_2} dt_1$.

If the transport occurs purely by incoherent stepwise hopping between neighboring wells, the $y$ charges can be grouped into pairs $(y_{2j-1}, y_{2j})$, and within each pair the two $y$ charges must have opposite signs so that the system returns to a diagonal state after every two transitions [21,22]. Each pair of $y$-charges can be thought of pictorially as a "dipole." The second step in the noninteracting-blip approximation is then to assume that all interdipole interactions are zero [4]. The NIBA has been found to be a very useful approximation in the case of the dissipative two-state system [4,8,9]. For the spin-boson model, the assumption of noninteracting dipoles is justified in several physically quite distinct limits and the NIBA seems to give accurate predictions between these limits. The essential difference between the two-state and the multistate system is that the multistate system will not always return to a diagonal state after every two transitions whereas the two-state system is forced to do so by the boundary conditions. Because of this difference, the NIBA may not necessarily yield a good approximation for the multistate dynamics in the same parameter region.

Now we summarize briefly the results of applying the NIBA to the multistate system [21,22]. Within the NIBA, the integrand of the generating functional factorizes into products of dipolar contributions. Realizing that all terms in Eq. (3.5) corresponding to $m \neq 1$ do not contribute to the second moment, we find from Eq. (2.17)

$$\langle q^2(t) \rangle = \Delta^2 \int_0^t d\tau\, e^{-Q(\tau)} (t - \tau) \,, \tag{3.6}$$

which in the large $t$ limit reduces to the golden rule result (3.1) with (3.2). Therefore, for a strict Ohmic spectral density [Eq.(2.7) with $\omega_c \to \infty$], the NIBA predicts a power-law temperature dependence $D \sim T^{2K-1}$ for all $K$ and $T$ [22]. The golden rule is manifestly the result of a perturbation theory to order $\Delta^2$. However, the above shows that the golden rule is actually equivalent to the NIBA, which rests on two assumptions: (1) the transport is incoherent, i.e., the tunneling path returns to a

diagonal state after every two transitions, and (2) the interdipole interactions are zero. These two assumptions are expected to be valid in the high temperature and/or strong dissipation limit.

For the case $K = 0$, assumption (1) is of course not satisfied, but assumption (2) is now exact. Because of this, Eq. (3.6) becomes *exact* for $K = 0$. A straightforward calculation for the bare system confirms that this is indeed true

$$\begin{aligned}\langle q^2(t)\rangle &= \sum_n n^2 \left|\langle n|e^{-itH_0/\hbar}|0\rangle\right|^2 \\ &= \sum_n n^2 |I_{|n|}(i\Delta t)|^2 \\ &= (\Delta t)^2/2 \,, \end{aligned} \tag{3.7}$$

where $I_n(z)$ is the modified Bessel function [27]. Consequently, the NIBA result (3.6) coincides with the exact mean squared displacement (3.7). We should emphasize here that for the bare system, transport is superdiffusive as indicated by Eq. (3.7). Under the usual definition for the diffusion coefficient, $D$ would be infinite.

Given that the NIBA is exact for $K = 0$ as well as being a good approximation for the incoherent (high $T$ and/or large $K$) limit, one may wonder if it would also provide a reasonable approximation for small-to-intermediate values of $K$ and low temperatures. One can answer this question by studying the $T = 0$ behavior of the diffusion coefficient for $0 < K < 1/2$. First, the golden rule result Eq. (3.2) implies that $D \to \infty$ as $T \to 0$. However, while the $\Delta^2$ contribution to $D$ in the golden rule diverges as $T \to 0$, the diffusion coefficient should go to zero for *all* $K > 0$. This expectation is based on the aforementioned duality between the tight-binding and the weak corrugation model [17,19]. Therefore the NIBA, while being exact for $K = 0$, must have a zero radius of convergence in $K$. Hence the NIBA must be qualitatively incorrect for small-to-intermediate values of $K$ at low temperatures, and this we will indeed observe from the QMC results described below.

## IV. STOCHASTIC METHOD FOR SAMPLING REAL-TIME PATH INTEGRALS

We have argued that the NIBA is not able to provide correct results for intermediate values of $K$ at low temperatures. To obtain results for this nonperturbative parameter region, we resort to Monte Carlo techniques. The MC method used to compute the diffusion coefficient is based also on the path-integral formula of Sec. II. To formulate the MC algorithm, we first "discretize" the paths by allowing transitions only at evenly spaced grid points on the time axis: $t_1, t_2, \ldots, t_N$, where $t_i = i\delta t$ and $\delta t = t/N$. For a numerical evaluation, $N$ has to be kept finite and convergence to the $N \to \infty$ limit will be verified at the end by carrying out the simulation for increasing values of $N$. After discretization, the influence functional becomes

$$\mathcal{F}[\{x_i\},\{y_i\}] = \exp\left(\sum_{j<k} y_k S_{kj} y_j + 2i \sum_{j<k} y_k R_{kj} x_j\right) , \tag{4.1}$$

where $S_{kj} = S(t_k - t_j)$ and $R_{kj} = R(t_k - t_j)$. The free action in Eq. (2.15) is given by a product of free short-time propagators

$$\exp \widetilde{S}_0[\{x_i\},\{y_i\}] = \prod_{j=1}^{N} G_0(x_j, y_j) \tag{4.2}$$

with

$$G_0(x,y) = I_{|x+y/2|}(i\Delta\delta t)\, I_{|x-y/2|}(-i\Delta\delta t) \,. \tag{4.3}$$

In the discretized version, we make use of the following expansion [27] of the modified Bessel function for small $|z|$,

$$I_n(z) \approx \frac{(z/2)^n}{n!} \tag{4.4}$$

in order to replace the exact free propagator by an $m$th order approximate propagator $G_0^{(m)} = G_0 + O(\delta t^{m+1})$. Table I gives explicitly the formula for a second-order ($m$=2) approximate propagator, but the respective expressions for other orders can be obtained in straightforward ways using Eqs. (4.3) and (4.4). In practice, it is sufficient to use $m = 2$.

The generating functional takes on the discretized form

$$Z(\lambda,t) = {\sum_{\{y\}}}' \exp\left(\sum_{j<k} y_k S_{kj} y_j\right) {\sum_{\{x\}}}'' \prod_j G_0^{(m)}(x_j, y_j) \exp\left[\lambda \sum_j x_j + 2i \sum_{j=1}^{N-1} x_j \sum_{k=j+1}^{N} R_{kj} y_k\right] , \tag{4.5}$$

where the prime on the $y$ configurational sum indicates that the sum over the $\{y_i\}$ charges is subject to the following constraints: (1) for every $i$, $y_i$ is an integer and $|y_i| \le m$ and (2) $\sum_{i=1}^{N} y_i = 0$. The double prime on the $x$ configurational sum indicates that the sum over the $\{x_i\}$ charges is subject to the following constraints: (1) for every $i$, $2x_i$ is an integer; (2) given $y_i$, $|x_i + y_i/2| + |x_i - y_i/2| \le m$; and (3) $\sum_{i=1}^{N} x_i$ is an integer. Then given any $\{y_i\}$ configuration, the sum over $\{x_i\}$ can be performed exactly giving

$$Z(\lambda,t)=\frac{\sum'_{\{y_i\}}\exp\left(\sum_{j<k}y_kS_{kj}y_j\right)\prod_j G^{(m)}[y_j,(\lambda+z_j)]}{\sum'_{\{y_i\}}\exp\left(\sum_{j<k}y_kS_{kj}y_j\right)\prod_j G^{(m)}(y_j,z_j)}, \tag{4.6}$$

where $G^{(m)}(y,z)=\sum''_x G_0^{(m)}(x,y)e^{xz}$ with

$$z_j=\begin{cases}2i\sum_{k=j+1}^{N}R_{kj}y_k, & j<N\\ 0, & j=N\end{cases}, \tag{4.7}$$

and the $G^{(m)}$ function for $m=2$ is given in Table II. The denominator in Eq. (4.6) is equal to unity and has been added to bring Eq. (4.6) into a form that is suitable for MC sampling.

Twice differentiating the generating functional in Eq. (4.6) with respect to $\lambda$ and taking the limit $\lambda\to 0$ finally yields the expression for the mean squared displacement

$$\langle q^2(t_M)\rangle = Z(0,t)^{-1}\sum_{\{y_i\}}{}'\exp\left[\sum_{j<k}y_kS_{kj}y_j\right]\prod_{i=M+1}^{N}G^{(m)}(y_i,z_i)\left[\sum_{j=1}^{M}G^{(m)\prime\prime}(y_j,z_j)\prod_{l=1\neq j}^{M}G^{(m)}(y_l,z_l)\right.$$
$$\left.+\sum_{j=1}^{M}\sum_{k=1\neq j}^{M}G^{(m)\prime}(y_j,z_j)G^{(m)\prime}(y_k,z_k)\prod_{l=1\neq j,k}^{M}G(y_l,z_l)\right], \tag{4.8}$$

where $Z(0,t)$ is just the denominator in Eq. (4.6), $G^{(m)\prime}(y,z)\equiv\partial G^{(m)}(y,z)/\partial z$, and $G^{(m)\prime\prime}(y,z)\equiv\partial^2G^{(m)}(y,z)/\partial z^2$. Notice that Eq. (4.8) applies to *all* intermediate times $t_M$ with $M\le N$, the number of discretizations. Consequently, all intermediate time points can be sampled simultaneously in one single simulation.

At this point, the stochastic sampling of the mean squared displacement should proceed in a straightforward manner following Eq. (4.8). The most obvious way to carry out the MC sampling is to use the factor $\exp\sum_{j<k}y_kS_{kj}y_j$ as the weight function and sample the configurations $\{y_i\}$, accumulating the rest of the factors in the numerator and the denominator separately. However, there is a problem with this approach — when the magnitude of the system-bath coupling is small, the factor $\exp\sum_{j<k}y_kS_{kj}y_j$ produces no weighting and hence the sampling is highly inefficient for small $K$. In view of this, one may then attempt to use the absolute value of the denominator as the weight (since the entire denominator is not necessarily positive definite). Unfortunately, there is another more subtle problem with this alternative approach.

TABLE I. Allowed values of $x_i$ corresponding to a given $y_i$ and the corresponding second-order approximate free propagators.

| $y_i$ | $x_i$ | $G_0^{(2)}(x_i,y_i)$ |
|---|---|---|
| 2 | $\pm1$ | $-(\Delta\delta t/2)^2/2$ |
| | 0 | $(\Delta\delta t/2)^2$ |
| 1 | $\pm1/2$ | $\pm i\Delta\delta t/2$ |
| 0 | $\pm1$ | $(\Delta\delta t/2)^2$ |
| | 0 | $1-2(\Delta\delta t/2)^2$ |
| $-1$ | $\pm1/2$ | $\mp i\Delta\delta t/2$ |
| $-2$ | $\pm1$ | $-(\Delta\delta t/2)^2/2$ |
| | 0 | $(\Delta\delta t/2)^2$ |

This difficulty arises when charge configurations that contribute to the numerator and denominator in Eq. (4.8) are almost mutually exclusive (a simple example is the case $K=0$). Using the absolute magnitude of the denominator as the weight causes ergodicity problem for the MC sampling, since most of the configurations that are important for the denominator may not contribute to the numerator. Fortunately, this problem can be solved by standard methods of importance sampling [28]. To this end, we first rewrite the Monte Carlo problem in the following schematic form

$$\langle q^2(t_M)\rangle=\frac{\sum'_{\{y_i\}}P_0A}{\sum'_{\{y_i\}}P_0B}\equiv\frac{\sum'_{\{y_i\}}P_0|A|\exp[i\arg(A)]}{\sum'_{\{y_i\}}P_0|B|\exp[i\arg(B)]}, \tag{4.9}$$

where $P_0$ represents the factor $\exp\sum_{j<k}y_kS_{kj}y_j$, $A=\sum_{j=1}^{N}G^{(2)\prime\prime}(y_j,z_j)\prod_{l\neq j}G^{(2)}(y_l,z_l)+\sum_{j\neq k}G^{(2)\prime}(y_j,z_j)\,G^{(2)\prime}(y_k,z_k)\prod_{l\neq j,k}G^{(2)}(y_l,z_l)$ and $B=\prod_{j=1}^{N}G^{(2)}(y_j,z_j)$ represent the remaining factors in the numerator and denominator, respectively. We can then reexpress Eq. (4.9) in the equivalent form

$$\langle q^2(t_M)\rangle=\left\langle\frac{A}{|A|+|B|}\right\rangle_P\Big/\left\langle\frac{B}{|A|+|B|}\right\rangle_P, \tag{4.10}$$

where the angular brackets denote averages over the weight function $P=(|A|+|B|)P_0$.

TABLE II. Definitions of the second-order $G$ functions.

| $y_i$ | $G^{(2)}(y_i,z)$ |
|---|---|
| $\pm2$ | $(\Delta\delta t/2)^2(1-\cosh z)$ |
| $\pm1$ | $\pm2i(\Delta\delta t/2)\sinh z/2$ |
| 0 | $1-2(\Delta\delta t/2)^2+2(\Delta\delta t/2)^2\cosh z$ |

Two types of Monte Carlo moves were used in the simulations. The first was a double charge Metropolis move involving a pair of charges moved in opposite directions in order to maintain the charge neutrality constraint $\sum_j y_j = 0$. These moves have relatively low acceptance ratio, especially for large $K$, generally less than 10%. The second type of MC move is a charge migration move in which two neighboring charges are exchanged, effectively translating charges along the chain. These moves have high acceptance ratio ($\approx 50\%$), but by themselves, they do not generate ergodic behavior. For the QMC simulation results presented here, anywhere from 10 000 to 100 000 samples were collected. Typically $N = 18$ to 30 discretizations were used for a maximum real time $\Delta t = 9.6$, and the code performs at an average speed of approximately 12 CPU minutes per 10 000 passes on an IBM RISC 6000 Model 580. In all of our calculations, we verify convergence by systematically increasing the discretization $N$ until the results do not vary by larger than the statistical error.

To conclude this section, we give a simple argument as to why this method is able to circumvent the sign problem. The crucial step is the transformation to sum and difference coordinates in Eq. (2.13). The $x(\tau)$ can be thought of as quasiclassical variables corresponding to the diagonal elements of the time-dependent reduced density matrix, whereas the $y(\tau)$ represents quantum fluctuations which are related to the off-diagonal elements of the density matrix [26]. (We note that a similar idea leads to the Wigner function formalism which has been applied to the dual weak corrugation model by Chen *et al.* [25].) With regard to the numerical treatment presented here, the fact that the quasiclassical paths can be integrated out analytically provides enormous advantage. As a result, we are left with a stochastic sampling over the quantum fluctuations alone and the influence functional then provides a natural weight for intermediate-to-strong damping. This method is related to the original filtering approach [7], but is much more useful for dissipative systems since it fully exploits the symmetry properties of the influence functional [21]. A similar algorithm can be used to compute the mobility of the dissipative multistate system, which is sketched in the Appendix.

## V. RESULTS AND DISCUSSIONS

In this section we present numerical results obtained from the dynamical simulations described in the preceding section. Figure 1 shows QMC results for the mean squared displacement $\langle q^2(t)\rangle$ as a function of time for the bare multistate system, $K = 0$. For the data shown in Fig. 1, $N = 24$ discretizations were used and 20 000 MC samples were collected, with five passes in between every pair of samples. As expected, the transport is superdiffusive, indicated by the $t^2$ dependence of the mean squared displacement. Figure 1 shows that the numerical results are in good agreement with the exact solution, indicated by the solid line.

Figure 2(a) shows typical results for the mean squared displacement for $K = 1/4$ at several temperatures $T$. For all temperatures studied, the mean squared displacement exhibits an inertial behavior at short times, but at longer times the transport becomes diffusive for all $K > 0$, and $\langle q^2(t)\rangle \sim t$. Figure 2(b) shows results for $K = 5/4$ and the same temperatures. A comparison between Figs. 2(a) and 2(b) reveals that for larger system-bath coupling $K$ (and/or higher temperatures), the diffusive behavior generally develops sooner. Also note the difference in the scales for $\langle q^2(t)\rangle$ in Figs. 2(a) and 2(b). The diffusion

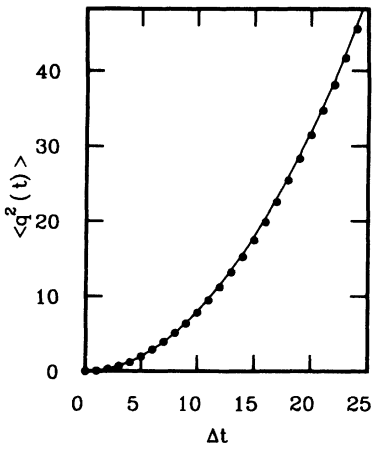


FIG. 1. Mean squared displacement $\langle q^2(t)\rangle$ for the bare multistate system ($K = 0$) generated by QMC simulations (circles). The solid line represents the exact result.

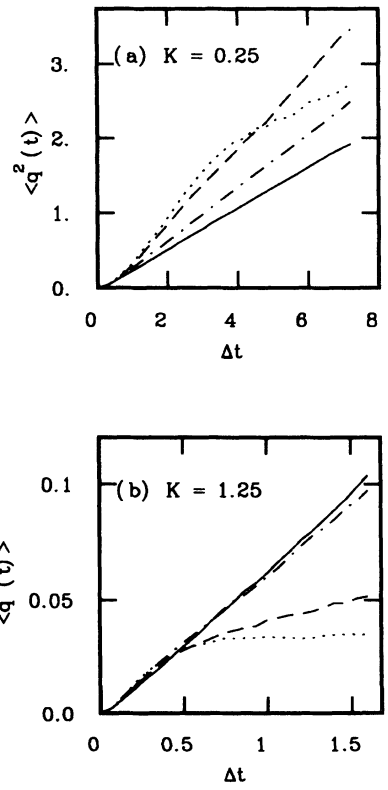


FIG. 2. Mean squared displacement for $\omega_c = 5\Delta$ and (a) $K = 1/4$ and (b) $K = 5/4$ at several temperatures: $k_B T/\hbar\Delta = 0.156$ (dotted line), 0.625 (dashed line), 2.5 (dot-dashed line), and 5 (solid line).

coefficient of the particle is in general smaller for larger $K$.

The mean squared displacement has been computed for a variety of system-bath coupling parameters $K$ at different temperatures. The resulting diffusion coefficients, obtained from the best linear fit to the tail of each mean squared displacement, are shown in Figs. 3(a)–3(e) for $K = 1/8$, $1/4$, $1/2$, $3/4$, and $7/8$ and in Figs. 4(a) and 4(b) for $K = 1$ and $5/4$. The solid line in each figure indicates the NIBA prediction for the diffusion coefficient. For all values of $K$, the diffusion coefficient is well approximated by the NIBA at high temperatures. This observation confirms the earlier assertion that for high temperatures, the transport proceeds entirely by incoherent tunneling between nearest-neighbor wells whose stepwise hopping rate is given by the golden rule formula for the truncated two-state system.

Although the NIBA works well for high temperatures, large deviations are observed at low temperatures for $K < 1$. The NIBA predicts that $D \sim T^{2K-1}$ as $T \to 0$, which would imply a divergent diffusion coefficient for $K < 1/2$. On the contrary, the MC results in Figs. 3(a) and 3(b) show clearly that for $K < 1/2$, $D$ goes to zero as $T \to 0$, and the diffusion coefficient exhibits a nonmonotonic temperature dependence. Starting from the high-temperature end, the diffusion coefficient increases with decreasing temperature and reaches a pronounced maximum, after which it decreases again with $T$, going to $D(T = 0) = 0$ approximately linearly with $T$ [21]. These results indicate that in the low-temperature region the NIBA (or the equivalent golden rule) are qualitatively incorrect.

For $1/2 < K < 1$, the NIBA again predicts that $D$ vanishes with a $T^{2K-1}$ power law as $T \to 0$. At first sight, the numerical results in Figs. 3(d) and 3(e) seem to suggest that the NIBA behavior may be correct for low temperatures. Unfortunately, the QMC data for the diffusion coefficient are not accurate enough at the low-temperature limit to prove or disprove the $T^{2K-1}$ power law. To decide whether it is correct in this region, we

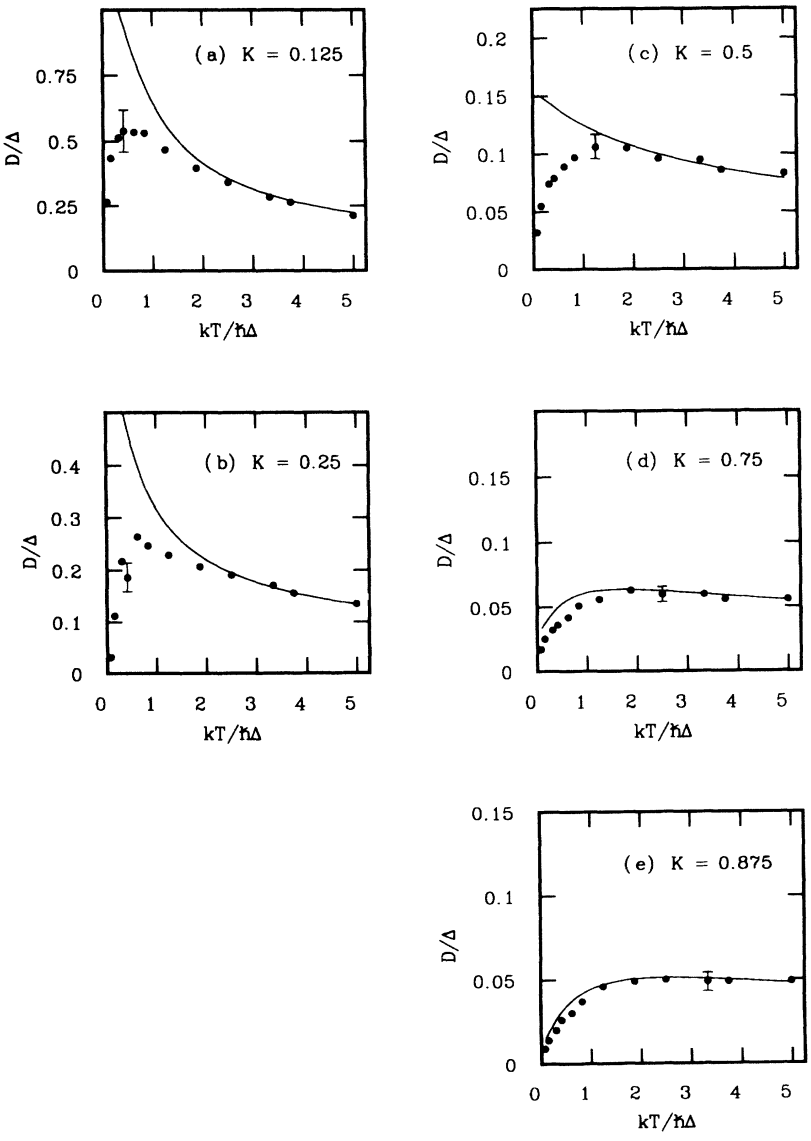


FIG. 3. Diffusion coefficient $D/\Delta$ (in units of $a^2$) extracted from the long-time portion of the mean squared displacement for $\omega_c = 5\Delta$ and (a) $K = 1/8$, (b) $K = 1/4$, (c) $K = 1/2$, (d) $K = 3/4$, and (e) $K = 7/8$ as a function of temperature $T$. Solid lines indicate the NIBA prediction. Note the change in scale as $K$ is increased.

refer to our earlier QMC results for the linear mobility $\mu_l$ [11]. Using the method outlined in the Appendix, the linear mobility for the same model has been computed at low temperatures for several values of $K < 1$. For all $K < 1$, it was found that $\mu_l$ has the universal low-temperature form [21]

$$\mu_l(T) = \mu_l(T=0) - dT^2 , \tag{5.1}$$

where $d$ is a nonuniversal positive prefactor. Combined with the Einstein relation $\mu_l(T) = D(T)/kT$, this implies that the asymptotic low-temperature behavior of the diffusion coefficient is of the form

$$D(T) = c_1 T - c_3 T^3 , \tag{5.2}$$

so that $D(T) \sim T$ as $T \to 0$ for all $K < 1$. Applying this result to the region $1/2 < K < 1$, we see that the perturbative result again predicts an incorrect low-temperature behavior of $D$, although it gives the correct limiting value $D(T \to 0) = 0$.

We note that the diffusion coefficient can be computed exactly in a nonperturbative manner at all temperatures for the special value $K = 1/2$ [21]. This analytical computation confirms the temperature dependence of $D$ as outlined above quantitatively and demonstrates the breakdown of the NIBA at low temperatures [29]. A simple estimate for the "Kondo temperature" $T_K$, which separates the perturbative from the nonperturbative region is given by $T_K = \hbar\Delta_{\rm eff}/k_B$, where $\Delta_{\rm eff} = \Delta(\Delta/\omega_c)^{K/(1-K)}$. For temperatures below $T_K$, the NIBA predictions are qualitatively incorrect. The Kondo temperature also provides a rough estimate for the position of the maximum of $D(T)$ in the region $0 < K < 1/2$.

Figures 3(d) and 3(e) show that for $1/2 \leq K < 1$, the maximum that existed for $K < 1/2$ has now almost disappeared. Indeed, the $T^{2K-1}$ power law should hold for arbitrarily high temperatures in the case of strict Ohmic damping ($\omega_c \to \infty$), and therefore, $D$ is expected to increase monotonically with temperature for $K > 1/2$. However, Figs. 3(d) and 3(e) show that a weak maximum remains even for $K > 1/2$. For a resolution of this apparent discrepancy, we note that a finite cutoff frequency $\omega_c$ has been used in the simulations and therefore the $T^{2K-1}$ law is modified by a universal $T^{-1/2}$ dependence for temperatures well above $\hbar\omega_c/k_B$ [24,30]. As a consequence, the (rather broad) maxima in Figs. 3(d) and 3(e) are most likely results of the finite cutoff frequency $\omega_c = 5\Delta$ employed in our study. We have performed additional simulations using a larger $\omega_c = 10\Delta$, and the MC results, shown in Figs. 5(a) and 5(b), indicate that the maximum has now completely disappeared from the temperature range studied. But with any finite $\omega_c$, at high enough temperatures the $T^{-1/2}$ tail will eventually set in again.

The MC results in Figs. 3(a)–(e) indicate that the NIBA predictions are accurate at high temperatures but grossly incorrect at low temperatures. This implies that while both assumptions of the NIBA are correct for high temperatures, at least one of the two assumptions is vio-

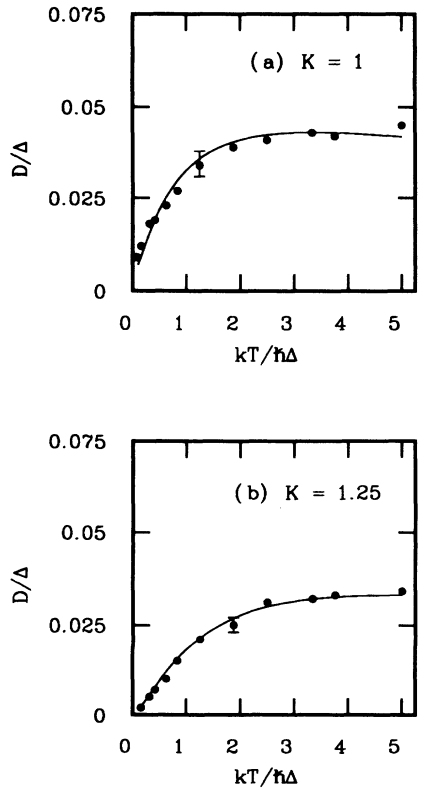


FIG. 4. The same as Fig. 3, but for (a) $K = 1$ and (b) $K = 5/4$.

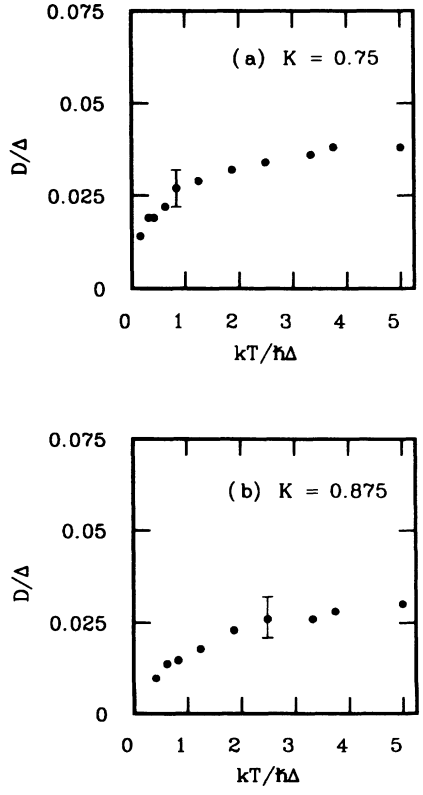


FIG. 5. The same as Fig. 3, but for (a) $K = 3/4$ and (b) $K = 7/8$ and a larger cutoff frequency $\omega_c = 10\Delta$. The maxima present in Figs. 3(d) and 3(e) for a smaller $\omega_c = 5\Delta$ are no longer present here.

lated for temperatures below $T_K$. One might then speculate on exactly why the NIBA fails for low temperatures. First, we note that our previous QMC results [7–9] for the spin-boson model indicate that the NIBA is quantitatively accurate for a (symmetric) two-state system with Ohmic dissipation in almost all parts of parameter space for a large enough cutoff frequency. In the case of a two-state system, the system must return to a diagonal state after every two transitions; hence the NIBA-assumption (1) is automatically satisfied. In view of this and the fact that the NIBA seems to be accurate for the two-state system, we would expect the NIBA to give reasonable results for the multistate system as long as assumption (1) is justified. Therefore our QMC results for temperatures below $T_K$ as well as earlier analytical calculations [19,21] suggest that assumption (1) is violated for the multistate system at low temperatures, implying that *the low-temperature transport is coherent for* $K < 1$. In other words, if the NIBA prediction is accurate for the two-state system in a particular region on the $T$-$K$ plane, then any deviation from the NIBA approximation for the multistate system in the same region on the $T$-$K$ plane indicates that the motion is coherent.

Next we briefly examine the QMC results for $K \geq 1$ shown in Figs. 4(a) and 4(b). Here the NIBA is essentially exact *for all temperatures* and the transport is always incoherent [22]. As temperature is increased from $T = 0$, the diffusion coefficient increases with the NIBA power law $D(T) \sim T^{2K-1}$; however, due to a finite cutoff frequency, $D(T)$ will exhibit a maximum around $T' \approx \hbar\omega_c/k_B$ (the exact value for $T'$ depends on $K$ as well), and finally decreases like $T^{-1/2}$ in the high-temperature end.

The MC results from Figs. 3 and 4 are summarized in Fig. 6 on the $T$-$K$ plane, in which we have used open diamonds to denote coherent transport and closed circles to denote incoherent transport, defined according to the criterion above. Since this criterion is a rather qualitative one, the phase diagram in Fig. 6 can only provide a rough estimate for the dynamic "phase transition" between coherent and incoherent transport. In addition, the results presented here were obtained for a finite cutoff $\omega_c = 5\Delta$, and the phase boundary may be somewhat different for a strict Ohmic bath. The Kondo temperature $T_K$ is shown as the solid curve in Fig. 6. $T_K$, as we have discussed previously, separates the nonperturbative region from the perturbative region, and it may be used as a crude estimate for the phase boundary. Clearly, there are discrepancies between this estimate and the coherent-incoherent boundary obtained from the QMC data. These discrepancies are certainly due to the *ad hoc* criterion we have employed to define the phase boundary and the finite cutoff used in the simulation. However, the qualitative picture emerging from our simulations is clear: for $K \geq 1$, the transport is incoherent for all temperatures, while for $K < 1$, the transport is coherent for low temperatures and eventually turns incoherent at a sufficiently high temperature.

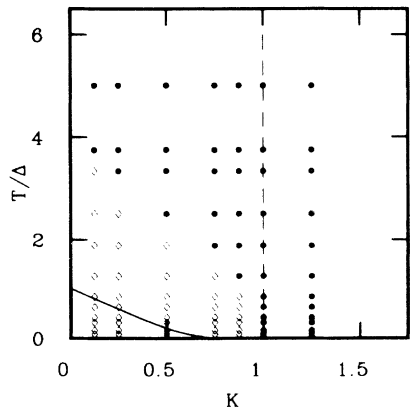


FIG. 6. Phase diagram for the coherent-incoherent transition for $\omega_c = 5\Delta$. Open diamonds indicate coherent transport and closed circles indicate incoherent transport (using the criterion discussed in the text). The dashed line indicates that above $K = 1$ the transport is incoherent for all temperatures. The solid line is the Kondo temperature $T_K$.

## VI. CONCLUSIONS

Real-time Monte Carlo methods have been used to study diffusion on a one-dimensional tight-binding lattice with Ohmic dissipation. The simulations confirm the overall picture for the behavior of the diffusion coefficient as a function of temperature and friction obtained from previous studies. For $0 < K < 1$, the transport is coherent at low temperatures and becomes incoherent at a sufficiently high temperature. For $K \geq 1$, the transport is always incoherent. In the incoherent region, the temperature dependence of the diffusion coefficient is well described by the noninteracting-blip approximation, which yields results identical to perturbation theory. The diffusion coefficient increases monotonically with temperature for $K > 1/2$ (provided the cutoff frequency is sufficiently large), whereas for $0 < K < 1/2$, the diffusion coefficient first rises with temperature, goes through a pronounced maximum, and then decreases with further increase in temperature. We believe that our simulation method provides a powerful approach to the study of transport properties of this model. Interesting (and straightforward) extensions of this work may be used to deal with the problem of a dissipative tight-binding model with more than one particle, or to study non-Ohmic dissipation and the effects of an external bias.

## ACKNOWLEDGMENTS

This work was supported in part by the Camille and Henry Dreyfus Foundation and the National Science Foundation (Grants No. CHE-9216221 and No. CHE-9257094). We thank Maura Sassetti and Ulrich Weiss for stimulating discussions.

## APPENDIX: QMC ALGORITHM FOR THE MOBILITY

In this appendix, we briefly summarize the stochastic algorithm for calculating the nonlinear mobility [11]. We

consider the same Hamiltonian (2), but now the external bias $\epsilon$ is nonzero. Again we assume that the system is prepared in a factorized initial state with the particle at $q = 0$. Under the bias, the particle will move in the direction of the gradient of the external field; in the long-time limit, the displacement of the particle $\langle q(t)\rangle$ grows linearly with $t$ and the mobility is defined by

$$\mu = \lim_{t\to\infty} \langle q(t)\rangle/\epsilon t. \tag{A1}$$

The time-dependent occupation probability is given by Eq. (2.15), but now the integrand is modified by an additional factor $\mathcal{C}[y(t)] = \exp[i\epsilon \int_0^t d\tau y(\tau)]$ due to the bias. With this, the generating functional $Z_\epsilon(\lambda, t)$ (the subscript is added to remind us that the external bias is nonzero) is given by Eq. (2.16) and the displacement is related now to the first moment of $Z_\epsilon(\lambda, t)$.

After transformation to the charge picture and the discretization, the generating functional takes on the same form as Eq. (4.5), but there is an additional factor

$$C_\epsilon(\{y_i\}) = \exp\left[-i\epsilon\delta t \sum_{j=1}^{N} j y_j\right] \tag{A2}$$

coming from the bias. Again, the $\{x_j\}$ charges can be traced out exactly since the bias-dependent factor does not contain any $x_j$. Equation (4.6) remains true, but with the factor $C_\epsilon(\{y_i\})$ appearing in the summand in both the numerator and the denominator. Differentiating this with respect to $\lambda$ gives the first moment for any intermediate time $t_M \le t$

$$\langle q(t_M)\rangle = Z_\epsilon(0,t)^{-1} {\sum_{\{y_i\}}}' \exp\left(\sum_{j<k} y_k S_{kj} y_j\right) \times C_\epsilon(\{y_i\}) \sum_{j=1}^{M}\left[G^{(2)\prime}(y_j, z_j) \times \prod_{l=1\neq j}^{M} G^{(2)}(y_l, z_l)\right], \tag{A3}$$

where $Z_\epsilon(0,t)$ is the denominator of Eq. (4.6) including the bias factor (A2). The Monte Carlo algorithm immediately follows from Eq. (A3) and can be written in the following schematic form:

$$\langle q(t_M)\rangle = \frac{{\sum}'_{\{y_i\}} P_0 A C_\epsilon}{{\sum}'_{\{y_i\}} P_0 B C_\epsilon}, \tag{A4}$$

where similar to Eq. (4.9) the factor $P_0$ again represents $\exp(\sum_{j<k} y_k S_{kj} y_j)$. Furthermore, $A$ and $B$ are the remaining bias-independent factors in the numerator and the denominator, respectively. Using the same importance sampling method described in Sec. IV, the first moment is expressed as the ratio of two stochastic averages over the distribution $P = (|A| + |B|)\, P_0$,

$$\langle q(t_M)\rangle = \left\langle \frac{A}{|A|+|B|} C_\epsilon \right\rangle_P \Big/ \left\langle \frac{B}{|A|+|B|} C_\epsilon \right\rangle_P . \tag{A5}$$

Note that in Eq. (A5) the distribution function is independent of the external bias $\epsilon$; therefore, the nonlinear mobility for any number of different $\epsilon$ can be computed from one single Metropolis trajectory. This feature allows one to conveniently compute the linear mobility $\mu_l$ (which is the $\epsilon \to 0$ limit of the nonlinear mobility) by calculating the nonlinear mobility for several values of $\epsilon$ in the same Monte Carlo simulation and then extrapolating to $\epsilon \to 0$.


[1] R.P. Feynman and A.R. Hibbs, *Quantum Mechanics and Path Integrals* (McGraw-Hill, New York, 1965).

[2] A.O. Caldeira and A.J. Leggett, Phys. Rev. Lett. **46**, 211 (1981); Ann. Phys. (N.Y.) **149**, 374 (1983); **153**, 445(E) (1983).

[3] R.P. Feynman and F.L. Vernon, Ann. Phys. (N.Y.) **24**, 118 (1963).

[4] A.J. Leggett, S. Chakravarty, A.T. Dorsey, M.P.A. Fisher, A. Garg, and W. Zwerger, Rev. Mod. Phys. **59**, 1 (1987).

[5] J. Kondo, in *Fermi Surface Effects*, edited by J. Kondo and A. Yoshimori, Springer Series in Solid State Sciences Vol. 77 (Springer, New York, 1988), and references therein.

[6] D. Chandler, in *Liquids, Freezing and Glass Transition*, 1991 Les Houches Lectures, edited by D. Levesque, J.P. Hansen, and J. Zinn-Justin (Elsevier, Amsterdam, 1991), pt. 1.

[7] C.H. Mak, Phys. Rev. Lett. **68**, 899 (1992).

[8] C.H. Mak and D. Chandler, Phys. Rev. A **41**, 5709 (1990); **44**, 2352 (1991).

[9] R. Egger and U. Weiss, Z. Phys. B **89**, 97 (1992).

[10] R. Egger and C.H. Mak, J. Chem. Phys. **99**, 2541 (1993).

[11] C.H. Mak, R. Egger, M. Sassetti, and U. Weiss (unpublished).

[12] V. Ambegaokar, U. Eckern, and G. Schön, Phys. Rev. Lett. **48**, 1745 (1982); U. Eckern, G. Schön, and V. Ambegaokar, Phys. Rev. B **30**, 6419 (1984).

[13] C.P. Flynn and A.M. Stoneham, Phys. Rev. B **1**, 3966 (1970).

[14] For a general overview, see Proceedings of the Fourth Conference on Muon Spin Rotations, Uppsala, 1986 [Hyperfine Interact. **31** (1986)].

[15] For a general review, see *Physics of Quantum Electron Devices*, edited by F. Capasso (Springer, New York, 1990).

[16] See, for example, D.N. Beratan, J.N. Betts, and J.N. Onuchic, Science **252**, 1285 (1991), and references therein.

[17] A. Schmid, Phys. Rev. Lett. **51**, 1506 (1983).

[18] F. Guinea, V. Hakim, and A. Muramatsu, Phys. Rev. Lett. **54**, 263 (1985).
[19] M.P.A. Fisher and W. Zwerger, Phys. Rev. B **32**, 6190 (1985); W. Zwerger, *ibid.* **35**, 4737 (1987).
[20] U. Eckern and F. Pelzer, Europhys. Lett. **3**, 131 (1987).
[21] U. Weiss and M. Wollensak, Phys. Rev. B **37**, 2729 (1988); U. Weiss, M. Sassetti, T. Negele, and M. Wollensak, Z. Phys. B **84**, 471 (1991).
[22] U. Weiss and H. Grabert, Phys. Lett. **108A**, 63 (1985).
[23] M. Sassetti, M. Milch, and U. Weiss, Phys. Rev. A **46**, 4615 (1992).
[24] C. Aslangul, N. Pottier, and D. Saint-James, J. Phys. (Paris) **47**, 1671 (1986).
[25] Y.-C. Chen, J. L. Lebowitz, and C. Liverani, Phys. Rev. B **40**, 4664 (1989).
[26] A. Schmid, J. Low Temp. Phys. **49**, 609 (1982).
[27] I.S. Gradsteyn and I.M. Ryzhik, *Tables of Integrals, Series, and Products* (Academic, New York, 1980).
[28] See, for example, J.P. Valleau and S.G. Whittington, in *Statistical Mechanics, Part A: Equilibrium Techniques*, Vol. 5 of *Modern Theoretical Chemistry*, edited by B.J. Berne (Plenum, New York, 1977).
[29] The analytical solution [21] for the diffusion coefficient at $K = 1/2$ was obtained under the assumption that $\Delta/\omega_c \ll 1$. Due to the finite $\omega_c = 5\Delta$ employed in our simulations, there are small deviations between our QMC data and the exact solution. Note also that in the limit $\Delta/\omega_c \ll 1$, the NIBA would predict a temperature-independent diffusion coefficient, whereas for our value of $\Delta/\omega_c$, there is a rather strong temperature dependence already in the NIBA prediction [solid line in Fig. 3(c)].
[30] R. Egger, C.H. Mak, and U. Weiss, J. Chem. Phys. (to be published).